GREEN'S FUNCTION TECHNIQUE IN FORMING INTENSIVE BEAMS

V. Ivanov

April 12, 2010

Muons, Inc., 522 N.Batavia Ave., Batavia, Illinois 60510, USA, vivanov@fnal.gov *received 29 July 2008*

revised Day Month 2008

Abstract

The numerical extensions of the Green's function thechnique have been used to represent a space charge of intensive beams in three-dimensional (3D) case. The introduced tri-linear approximation helps to avoid the numerical noise of space charge density on the beam boundary, peculiar to the commonly used piecewise-constant approximation. Both artificial and real singularities for the potential and field gradients have been analyzed. The efficiency of the suggested numerical algorithms has been demonstrated by benchmark tests. The design of the electron gun for an X-band sheet-beam klystron has been done using these algorithms. *Keywords: Green's function; beam optics; klystron gun.* PACS numbers:

29.27.Bd

1 Introduction

One of the most powerful tools to solve mathematical physics problems is the Green's function method. The importance of this method is that it occupies an intermediate place between purely numerical and analytical methods. Thus, an arbitrary-order derivative can be evaluated analytically, when the solution of the initial-boundary problem is represented as an integral convolution of the field source density with the Green's function. In this case, evaluation of derivatives is performing with no accuracy loss in contrast to using the correspondent numerical scheme. The algorithms and numerical results presented in this paper stem from the earlier works of the author [1]-[3]. Some other computationally fast approaches based on the Green's function formalism (so-called "templates") have been developed [4]-[5], such as the analytical representation of the field of an ellipsoidal bunch [6]. They drastically decrease the calculation time in the case of ultra relativistic bunches in accelerating structures.

2 Analytical technique for evaluation of a space charge potential in 3D

The potential of the electrostatic field of electrodes and space charge of the beam can be represented by a sum of a single-layer potential of surface sources σ and volume potential of sources ρ

$$\phi(x_0, y_0, z_0) = \int\limits_S \sigma(x, y, z) G(x_0, y_0, z_0; x, y, z) dS + \int\limits_V \rho(x', y', z') G(x_0, y_0, z_0; x, y, z) dV, \ (x, y, z) \in S, \ (x', y', z') \in V. \quad (1)$$

Applying the boundary conditions to the integral representation (1), one can get an integral equation for the field source σ. The continuity equation

$$div\vec{j} = 0, \ \vec{j} = \rho\vec{v} \quad (2)$$

with the initial values for the emission current

$$\vec{j}|_{S_0} = \vec{j_0} \quad (3)$$

on the emitter surface S_0, gives an equation for the space charge ρ, but the motion equation

$$\dot{\vec{p}} = Z(\vec{E} + [\vec{v} \times \vec{B}], \ \vec{E} = -\nabla\phi, \ \vec{p} = \frac{m\vec{v}}{\sqrt{1 - (v/c)^2}} \quad (4)$$

yields the velocity v of a particle with a charge Z and rest mass m. Here c is the speed of light in vacuum.

The magnetic field B includes as an external magnetic field B_0 of solenoids or permanent magnets as the self-consistent field of a relativistic beam

$$\vec{B}(\vec{r}) = \frac{4\pi}{\mu_0} \int\limits_V \frac{[\vec{j}(\vec{r}') \times \vec{v}(r')]}{|\vec{r} - \vec{r}'|^3} dV, \ \vec{r}' \in V, \quad (5)$$

where μ_0 is a permeability of vacuum.

The equations (1)-(5) is a complete set of non linear equations for the functions σ, ρ, v and B.

In the 3D case the analytical integration over a brick-type element can be done analytically also. Let us introduce a rectangular mesh $\{x_i\} \times \{y_j\} \times \{z_k\}$, and a space charge distribution approximated by a tri-linear form

$$\begin{aligned} \rho(x, y, z) \quad = \frac{1}{h_x h_y h_z} \{ & [(\rho_{i+1,j,k}(x - x_i) + \rho_{i,j,k}(x_{i+1} - x)) (y_{j+1} - y) + \\ & (\rho_{i+1,j+1,k}(x - x_i) + \rho_{i,j+1,k}(x_{i+1} - x)) (y_{j+1} - y)] (z_{k+1} - z) + \\ & [(\rho_{i+1,j,k+1}(x - x_i) + \rho_{i,j,k+1}(x_{i+1} - x)) (y_{j+1} - y) + \\ & (\rho_{i+1,j+1,k+1}(x - x_i) + \rho_{i,j+1,k+1}(x_{i+1} - x)) (y_{j+1} - y)] (z - z_k) \} . \end{aligned} \quad (6)$$

Then the potential of this charge distribution can be represented by an integral

$$\phi(x_0, y_0, z_0) = \sum_{i,j,k} \int\limits_{x_i}^{x_{i+1}} \int\limits_{y_j}^{y_{j+1}} \int\limits_{z_k}^{z_{k+1}} \rho(x, y, z) G(x_0, y_0, z_0; x, y, z) dxdydz, \tag{7}$$

where the Green's function of a point source is described by a formula

$$G(x_0, y_0, z_0; x, y, z) = \frac{1}{4\pi\varepsilon_0 \sqrt{(x - x_0)^2 + (y - y_0)^2 + (z - z_0)^2}} \equiv \frac{1}{4\pi\varepsilon_0 R}. \tag{8}$$

Here R is a distance between an observation point (x_0, y_0, z_0) and a source point (x, y, z) , and ε_0 is the vacuum permittivity.

Accordingly the potential evaluation can be reduced to evaluation of 4 integrals

$$\begin{aligned} I_1 &= \int\int\int \frac{xdxdydz}{R},\ I_2 = \int\int\int \frac{xydxdydz}{R}, \\ I_3 &= \int\int\int \frac{xyzdxdydz}{R},\ I_4 = \int\int\int \frac{dxdydz}{R}, \end{aligned} \tag{9}$$

and the other integrals can be expressed through these by cyclic replacement of variables x, y and z. Using linear replacement of variables $\hat{x} = x - x_0,\ \hat{y} = y - y_0,\ \hat{z} = z - z_0$ and a contraction $r = \sqrt{x^2 + y^2 + z^2}$ these integrals can be evaluated analytically

$$\begin{aligned} J_1 \quad &= \int\int\int \frac{xdxdydz}{r} = \frac{y}{4}\left[rz + (x^2 + y^2)\ln|z + r|\right] + \frac{z^3}{6}\ln|y + r| + \\ &\frac{x^2}{2}\left[z\ln|y + r| + y\ln|z + r| - z + xtg^{-1}\left(\frac{z}{x}\right) - xtg^{-1}\left(\frac{zy}{xr}\right)\right] + \\ &\frac{1}{36}\left[6x^2z - 2z^3 + 3zyr + 6x^3\left(tg^{-1}\left(\frac{zy}{xr}\right) - tg^{-1}\left(\frac{z}{x}\right)\right) - 3y(y^2 + 3x^2)\ln|z + r|\right], \end{aligned} \tag{10}$$

$$J_2 \quad = \int\int\int \frac{xydxdydz}{r} = \frac{zr^3}{12} + \frac{3}{24}(x^2 + y^2)[zr + (x^2 + y^2)\ln|z + r|, \tag{11}$$

$$J_3 \quad = \int\int\int \frac{xyzdxdydz}{r} = \frac{r^5}{15}, \tag{12}$$

$$\begin{aligned} J_4 \quad &= \int\int\int \frac{dxdydz}{r} = xy\ln|z + r| + yz\ln|x + r| + xz\ln|y + r| + \\ &-\frac{1}{2}\left[x^2tg^{-1}\frac{yz}{xr} + y^2tg^{-1}\frac{xz}{yr} + z^2tg^{-1}\frac{xy}{zr}\right]. \end{aligned} \tag{13}$$

The last integral was evaluated analytically at [7], but the result was done in complex form, not appropriate for direct utilization. That result also has errors.

Electric field components $\vec{E} = -\nabla\phi$ can be evaluated as the derivatives of the potential, for example,

$$E_z(x,y,z) \equiv -\frac{\partial}{\partial z}\phi(x,y,z) = \sum_{i,j,k} \int_{x_i}^{x_{i+1}} \int_{y_j}^{y_{j+1}} \int_{z_k}^{z_{k+1}} \rho(x,y,z)\frac{\partial}{\partial z}G(x_0,y_0,z_0;x,y,z)dxdydz. \quad (14)$$

The following set of integrals needed for this case

$$J_{1z} = \int\int \frac{dxdy}{r} = -ztg^{-1}\left(\frac{xy}{zr}\right) + y\ln|x+r| + x\ln|y+r|, \quad (15)$$

$$J_{2z} = \int\int \frac{xdxdy}{r} = \frac{1}{2}\left[yr + (x^2+z^2)\ln|y+r|\right], \quad (16)$$

$$J_{3z} = \int\int \frac{zdxdy}{r} = zJ_{1z}, \quad (17)$$

$$J_{4z} = \int\int \frac{xydxdy}{r} = \frac{1}{3}r^{3/2}, \quad (18)$$

$$J_{5z} = \int\int \frac{xzdxdy}{r} = \frac{z}{2}\left[yr + (x^2+z^2)\ln|y+r|\right], \quad (19)$$

$$J_{6z} = \int\int \frac{xyzdxdy}{r} = \frac{z}{3}r^{3/2}. \quad (20)$$

3 Singularity problems

Actually, the potential of an electric field is a regular limited function in all space, so the logarithmic terms in formulas 10-13, 15-19 produce artificial singularities, which must be excluded in program implementation. Furthermore the field gradients have real singularities on the vertices and edges of cubic cells at the beam boundary (point "a") [8]. Those singularities result in numerical noise, leading to artificial halo formation around the beam etc. All these singularity problems have been successfully overcome by using a high-order approximation for the space charge density [1]. The space charge distribution and its approximations are presented in Fig.1.

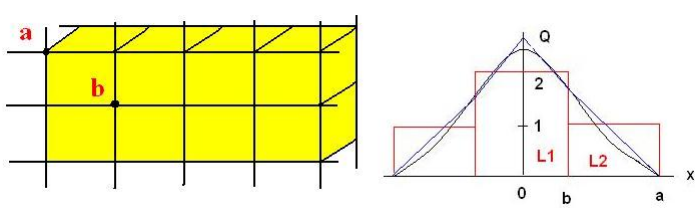

Figure 1: On the field singularity of charged cubic cells.

Both integrals over elements $L1$ and $L2$ have singularities at the point "'b". These integrals should be weighted with coefficients $Q1$ and $Q2$ associated with

the elements in the electric field evaluation. As a result singular terms are compensated at internal points of the beam for any smooth approximation, where $Q1 = Q2$, but they keep the singularity for a piecewise constant approximation where $Q1 \neq Q2$. The electric field at the boundary point $x = b$ has no singularity for smooth approximations because the singular integrals over element $L2$ are multiplied by $Qb = 0$. The singularity occurs for a piecewise constant approximation because the space charge coefficient $Q2 \neq 0$ this case.

4 Benchmark results

One of simplest test is the potential of a sphere of radius R with uniformly distributed total charge Q. In that case the charge density $\rho = \frac{3Q}{4\pi R^3}$, and the exact solution for potential is given by the formula

$$\phi(r) = \begin{cases} q\left[\frac{(R^2-r^2)}{2} + \frac{1}{r}\right] & r < R, \\ \frac{Q}{R} & r > R. \end{cases} \tag{21}$$

Actually a discrete set of charged cubes can represent this sphere. We put $R = 1$ and $Q = 1$ in our tests, and we use a uniform mesh for space charge in each direction. We will compare this exact solution with the analytical integration for piecewise-constant and linear approximations of space charge. In addition the numerical integration over the brick element is used

$$\phi_\diamond = \sum_i^n \sum_j^n \sum_k^n a_i a_j a_k \frac{\rho(x_i, y_j, z_k)}{\sqrt{(x_x - x_0)^2 + (y_j - y_0)^2 + (z_k - z_0)^2}}, \tag{22}$$

where a_i, a_j, a_k - weights, and x_i, y_j, z_k - nodes of Gaussian quadrature in 3D of order n. We will use $n = 2$ in our simulations, so this is an 8-node formula, which is quite enough for our goal.

Figure 2 shows the potential distribution for exact solution and for different integration schemes.

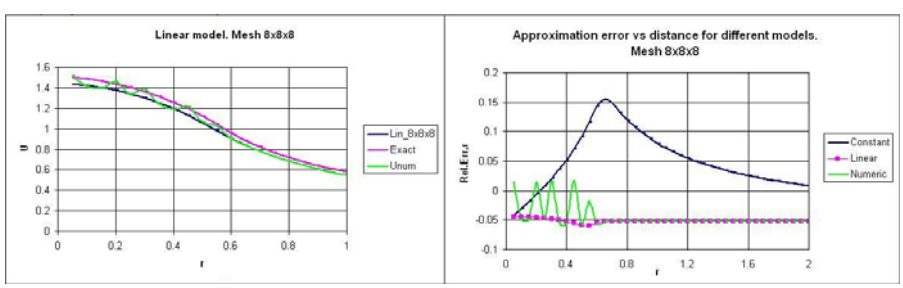

Figure 2: Left: Exact solution for a potential distribution (magenta), analytic integration (blue) and numerical integration (green). Right: relative error for different integration schemes.

One can see the oscillations in the numerical integration for the 'near' zone. That is because our quadrature formula does not take into account the singularity of the integrand function. It has a good accuracy in the "far" zone. The right graph in Figure 2 demonstrates a substantial difference in accuracy of computations between piecewise-constant and linear approximations.

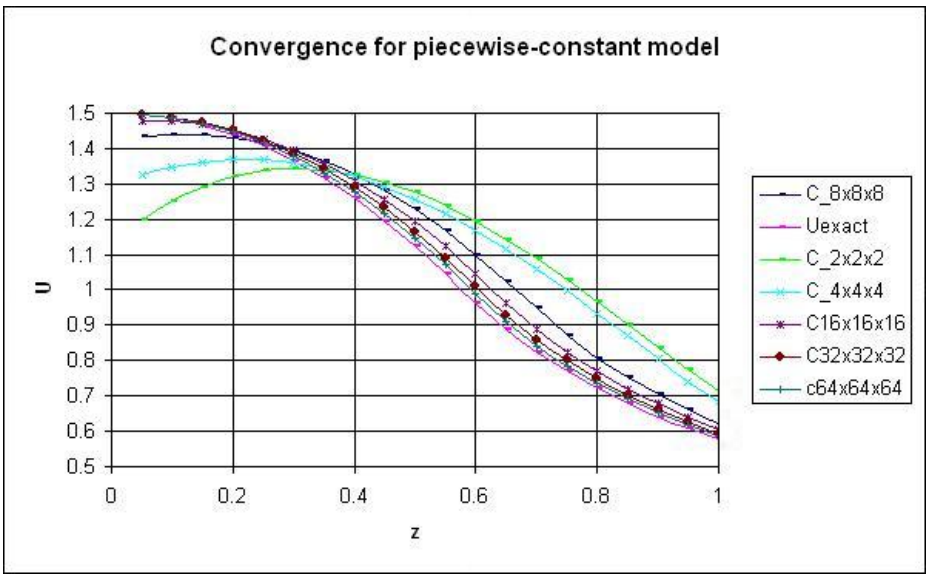

Figure 3: Exact solution for the potential of sphere (magenta), and analytic integration for the piecewise-constant model in a mesh refinement.

Figures 3 and 4 demonstrate the convergence rate for both approximations in varying of number of mesh cells in each direction from 2 to 64.

Figures 5 and 6 shows the convergence rate for both models and the run time dependence in a mesh refinement.

5 The adaptive algorithm of integration

One can see that numerical integration is the fastest computational algorithm, compared with both analytical schemes, but it has low accuracy near to the field-source region. The idea of an adaptive integration scheme is to combine the numerical and analytical approaches, and switch from the analytical scheme in near region to the numerical one in the far zone. The criterion for this switch is a relative distance from the field source compared to the dimension of the source.

Figure 7 demonstrates how it works for the example of a very coarse mesh of 2 x 2 x 2 cells representing a sphere. The left part of this picture corresponds to the criterion $r = 2.2$. It is close to a sphere of radius $R = 1$, and it produces

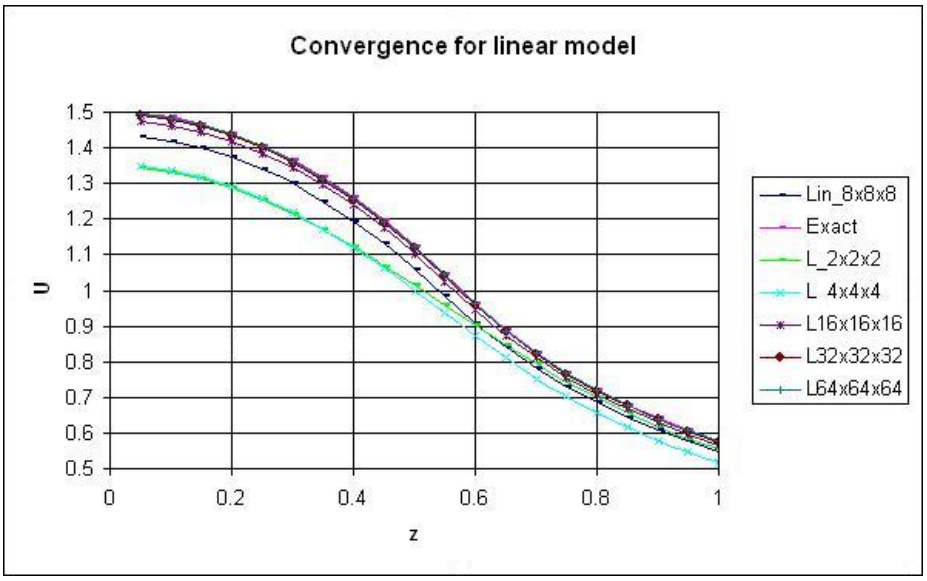

Figure 4: Convergence of analytical integration for a linear approximation of the space charge distribution.

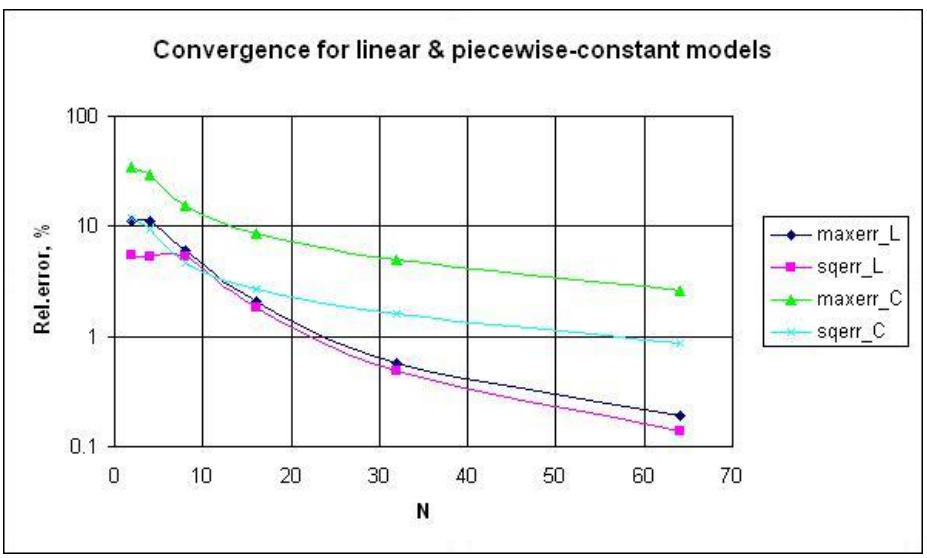

Figure 5: Maximal and mean square errors for piecewise-constant and linear models vs. the number of nodes in each direction

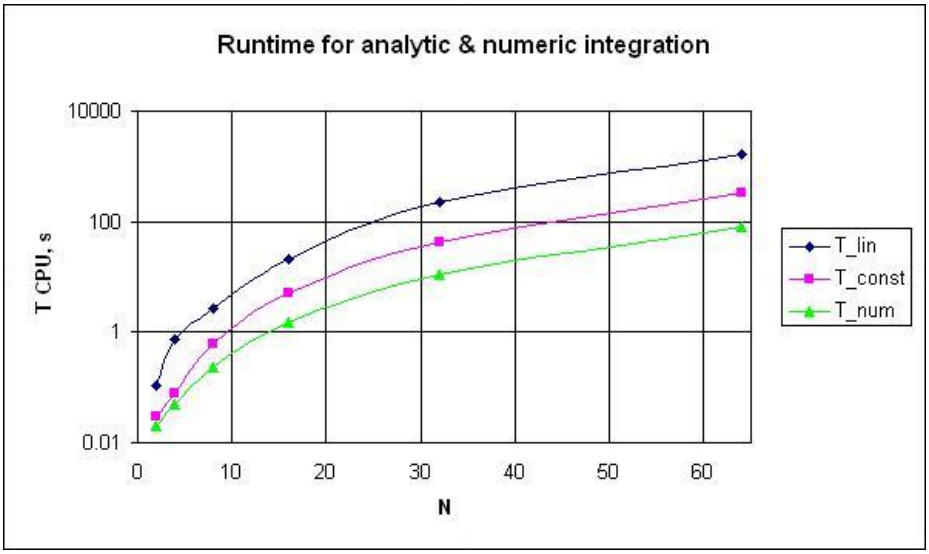

Figure 6: CPU-time for piecewise-constant and linear models vs. the number of mesh nodes in each direction

a reasonably large jump in the inter face region. The right picture shows very smooth passage from one algorithm to the other.

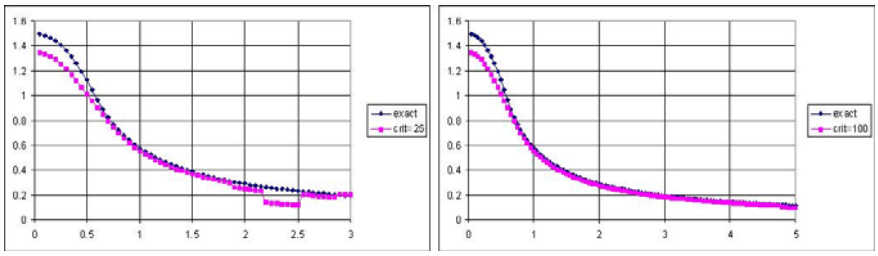

Figure 7: Worse mesh 2x2x2 cells shows clear the influence of the adaptation criterion

Figure 8 demonstrates that such a smooth inter face can be reached for a small value of the switch criterion, when the mesh is fine enough.

6 Sheet-beam gun design

Our simulations of beam optics for a sheet beam gun for an X-band klystron is an example of a realistic design. This type of gun is able to overcome the power limitations peculiar to the classical axially-symmetric klystron guns. Here the electron beam emitted from a cylindrically-shape cathode is compressed in one

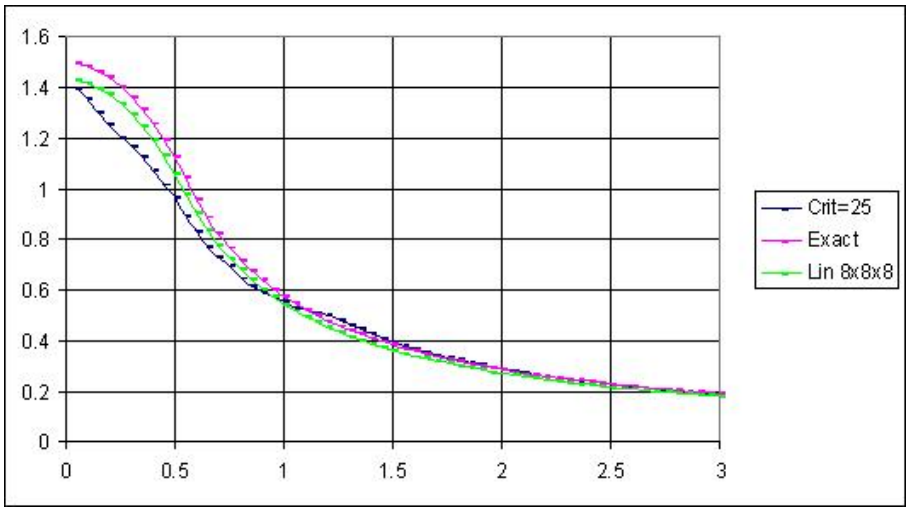

Figure 8: The adaptive integration algorithm can reduce the run time dramatically (factor of 5-10) with accuracy lost of about 0.5-1%

transverse direction, and is almost parallel in the other. As a result we get a sheet beam in the anode slot. The effect of space charge repulsion is much less in this gun compared with a cylindrical beam.

Figure 9 shows the geometry shape of anode and cathode assemblies, and the geometry model with triangular surface elements.

Figure 9: Parts, assembly and geometry model of a sheet-beam gun

Figure 10 demonstrates the results of a computer simulation for beam optics. It takes 10 iterations on space charge to reach a convergence of about 1 % for a total beam current on a mesh of 10,000 brick elements. The total simulation time was 65 minutes with a desktop PC 1.4 GHz.

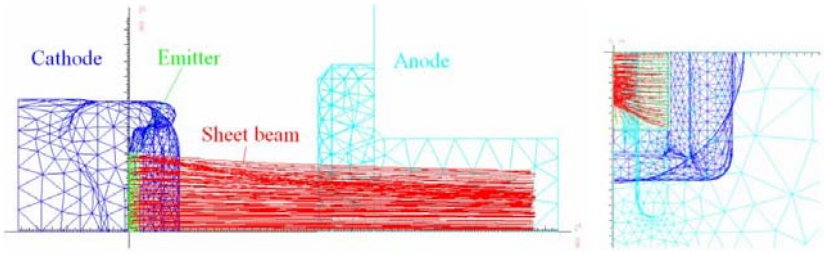

Figure 10: Beam optics for a sheet-beam gun of X-band klystron.

Acknowledgments

Special thanks to Dr. L.Vorobiev and Dr. P.Lucas for the fruitful discussion and criticism.

References

[1] V.Ivanov. Numerical methods for analysis of 3D non stationary flows of charged particles, 15. Trudy Instituta Matematiki, Izd-vo "Nauka", Sibirskoe Otdelenie, 1989.-p.172-187.

[2] V. Ivanov, A. Krasnykh, Analytical computations in solution of 3D problems of physical electronics by BEM//ACES-2002, March 18-22, 2002, Monterey, CA.

[3] V. Ivanov, A. Krasnykh, G. Scheitrum, D. Sprehn, L. Ives, G. Miram, 3D Modeling Activity for Novel High Power Electron Guns at SLAC, PAC-2003, May 12-16, 2003, Portland, USA.

[4] L.G.Vorobiev, R.C.York, High Current Beam Simulation using Templates $< http://cern.ch/AccelConf/e02/PAPERS/WEPLE092.pdf >$, EPAC 2002, Paris.

[5] L.G.Vorobiev, R.C.York, Calculation of longitudinal fields of high-current beams in the vicinity of conducting chambers, PAC'99, March 29th-April 2nd, pp.2781-2783, New York, 1999.

[6] M.Krasilnikov, Space charge algorithm for the multi ensemble model, Nucl. Instr. & Meth. in Phys. Research, A **558**(2006)69-73.

[7] Ji Quang, S.Lidia, R.Ryne, C.Limborg-Deprey, Three-dimensional quasi static model for high brightness beam dynamic simulation, Phys.Rev. Special Topics - Accel.& Beams, 9, 044204 (2006).

[8] G. Fikera, Uspekhi mat. nauk. 1975. T. 30. Vyp. 3. S. 105-124.